Very Long Transient Oxidation of a Nickel-based Single-Crystal Superalloy at 900 °C and 850 °C

Martin Batiste, Thomas Perez, Tom Sanviemvongsak, Clara Desgranges, Daniel Monceau

High Temperature Corrosion of Materials
https://doi.org/10.1007/s11085-024-10261-y

ORIGINAL PAPER

Very Long Transient Oxidation of a Nickel-based Single-Crystal Superalloy at 900 °C and 850 °C

Martin Batiste[1] · Thomas Perez[2] · Tom Sanviemvongsak[2] · Clara Desgranges[2,3] · Daniel Monceau[1]

Received: 11 July 2024 / Revised: 11 July 2024 / Accepted: 17 July 2024

Abstract

The isothermal oxidation of Ni-base single-crystal superalloy AM1 was investigated for up to 3600 h at 850 °C and 900 °C. The aim of the study was to test an existing model of oxidation kinetics that considers transitory oxide growth. The samples were characterized at various intervals to correlate the microstructure of the oxide scale with the oxidation kinetics. Transition alumina (θ) was observed among other transition oxides such as spinel, rutile, and chromia, which helped in understanding the nature and kinetics of the transitory stage. After a sufficiently long duration, all samples formed a continuous α-alumina layer at the metal/oxide interface. The previously published model, based on three kinetic parameters, was validated in the temperature range of 800–1200 °C. The duration of the transient regime characterized in this study at 850 °C and 900 °C was consistent with the kinetics model, with a slight increase in the value of the model parameter describing the lateral growth kinetics of α-alumina. This modification resulted in a slight reduction in the duration of the transient regime at low temperatures.

Keywords AM1 · Superalloy · High temperature oxidation · Transient oxidation · Oxidation kinetics

Introduction

Ni-base superalloys for turbine blades are designed to resist oxidation at 1100 °C and higher temperatures for thousands of hours. However, transient oxides with high growth kinetics form at intermediate temperatures and durations instead of α-alumina. Only a few data below 1000 °C are available in the literature. Predicting transient oxidation kinetics is crucial as it controls the depth of depletion of the γ' precipitates and, ultimately, the reduction of mechanical properties of the parts. In 2022, Perez et al. developed an oxidation model for AM1 (a first-generation

Extended author information available on the last page of the article

Published online: 27 July 2024

Ni-based single-crystal superalloy) that accounts for transient oxidation and can predict oxidation kinetics for all durations in the temperature range of 800–1200 °C [1]. The study highlighted the significance of the transient oxidation regime, particularly at lower temperatures within the range. The model confirmed the excellent oxidation resistance of the uncoated alloy. The model revealed that oxidation kinetics transitioned from values typical of spinel oxide growth to those typical of α-alumina. The oxide scale consists of a layer of α-Al_2O_3 at the metal/oxide interface, topped by a spinel layer with some chromia, and the presence of a Ta-rich rutile layer at the interface between the two layers or rutile grains within the spinel layer. This structure resembles that observed in other Ni-based superalloys. The duration of the transitory stage is governed by the lateral growth of alumina precipitates at the metal/oxide interface until the formation of a protective continuous layer of α-alumina. This phenomenon was observed by Perez et al. at high temperatures (> 900 °C). However, with decreasing temperatures, the transient regime was predicted to extend to very long durations, and the experiments conducted were too short to observe the formation of a protective alumina scale.

The parameters of the model were determined using isothermal thermogravimetric analysis (TGA). The results were also compared with stepwise multi-temperature TGA (SMT-TGA). Although these experiments facilitated the construction of a model for predicting oxidation kinetics, there was a lack of experimental data for long exposures at the lowest temperatures within the range. Since uncoated parts can be exposed to these intermediate temperatures (800–900 °C) for extended periods, augmenting the model with more experimental data was crucial for validating the model and enhancing its accuracy. Recently, Martin et al. reported the presence of both α and θ alumina on AM1 after oxidation below 950 °C [2]. Therefore, particular attention was paid in the present work to differentiate the various allotropic forms of alumina, even as internal oxides, as transient alumina is known to grow with a parabolic constant about two orders of magnitude higher than α-alumina.

The model by Perez et al. was developed using TGA, which are technically complex to maintain for extended periods. Therefore, the results presented in this work were obtained using box furnaces. Isothermal tests, with several samples weighed at various points during the test, were conducted for up to 3600 h at both 850 °C and 900 °C in laboratory air to enrich the database. The nature of the oxides formed at different durations was investigated using low-incidence *X*-ray diffraction (XRD), PSL spectroscopy, and scanning electron microscopy (SEM).

Experimental Procedures

Samples were cut from the same cylinder of AM1 alloy as in the previous study [1] (composition in Table 1). The bar underwent full heat treatment, including homogenization at 1300 °C for 3 h, aging at 1100 °C for 5 h, and further aging at 870 °C for 16 h. Two different geometries were employed: a flat cylinder with a diameter of 24 mm, providing a large surface area to minimize errors in net mass gain measurement, and parallelepipedic samples measuring 10 × 8 mm, intended for destructive SEM observations and photo-stimulated luminescence (PSL) spectroscopy.

Table 1 The chemical composition of AM1 is in ppm for Hf and S, and in % for other elements (data provided by Safran Aircraft Engines)

	Ni	Ta	Cr	Co	W	Al	Mo	Ti	Hf (ppm)	S (ppm)
wt%	Bal	7.97	7.54	6.61	5.49	5.2	2.01	1.2	460–490	0.104–0.123
at%	Bal	2.65	8.74	6.76	1.80	11.61	1.26	1.51	155–165	0.195–0.231

Impurities were analyzed using Glow Discharge Mass Spectrometry, while other elements were analyzed using *X*-ray fluorescence

The sample thicknesses varied from 0.5 to 0.9 mm. All samples were drilled for mounting on an alumina rod supported by a refractory brick. Subsequently, each sample underwent grinding with P600 grit surface finish on all surfaces, followed by degreasing in acetone and ethanol in an ultrasonic bath before being weighed.

Three parallelepipedic samples and one cylinder were oxidized in ambient air in two furnaces (Carbolite CWF 1300) with natural convection. Temperatures were set at 850 °C and 900 °C using a type K control thermocouple. At specified intervals (after 4 h, 50 h, 500 h, 980 h, 1800 h, 2500, 3004, 3600 h at 850 °C and after 1 h, 4 h, 16 h, 47, 107 h, 250 h, 490 h 775 h, 1600 h at 900 °C), samples were removed from the furnace and weighed. For certain durations, the samples underwent further characterization with XRD on a Bruker D8 GIXR using Cu-Kα radiation, with a step size of 0.02°, an angle of incidence of 10°, and a scan step time of 2 s in the 2θ range from 10° to 90°. At the conclusion of the test, or at certain intervals for the small parallelepipedic samples, they were sectioned for cross-section characterizations. Electrochemical deposition of copper was performed to prevent damage to the oxide scales during cutting. Backscattered electron (BSE) images were acquired using a SEM FEI Quanta 450 equipped with an EDS detector Bruker Quantax (SDD). PLS spectroscopy was also conducted on some cross sections using a Raman Jobin Yvon Horiba LabRAM HR Evolution, equipped with a 532 nm laser.

Results

The mass gains per unit area over exposure time at 850 °C and 900 °C are depicted in Fig. 1a. The same curves, as a function of the square root of time, are presented in Fig. 1b. Additionally, the oxidation kinetics calculated from the parabolic rate constants for α-Al_2O_3 growth on β-NiAl [3], and for Cr_2O_3 growth on Ni-30Cr [4], are provided as references. Our data lie between these references. For short durations, the mass gain curves of AM1 closely resemble the kinetics of chromia scale growth, whereas for longer durations, the mass gain curves plateau, and the rate of mass gains becomes similar to the kinetics of α-Al_2O_3 scale growth. This trend aligns with the observation that AM1 oxidation exhibits a transient regime of oxidation with oxide growth kinetics similar to chromia scale growth, before transitioning to the low oxidation kinetics typical of α-Al_2O_3 scale growth.

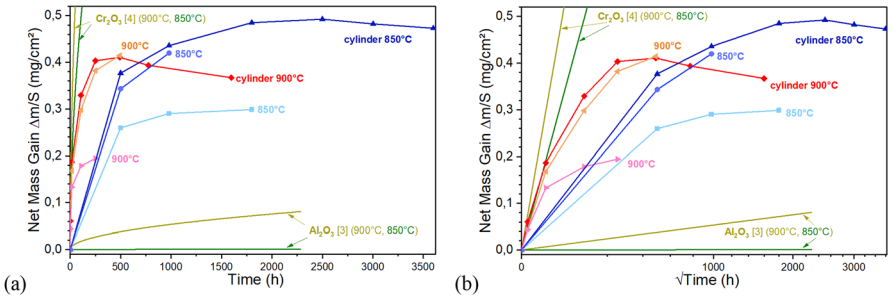

Fig. 1 Net mass gain curves **a** versus time **b** versus square root of time

The samples subjected to the longest durations at both temperatures are the two large flat cylinders. At 900 °C, the curves exhibit a rapid increase in mass gain, followed by a slowdown around 100 h, and eventual stabilization after 250 h, suggesting a duration of transient regime of about 300 h at 900 °C. For these samples, a slight decrease in mass is then observed until the end of the test. At 850 °C, the curve's shape is similar, but the transient regime appears to last longer, approximately 1500 h. Interestingly, the maximum net mass gain at 850 °C is higher than that at 900 °C. This behavior may seem surprising, but it is related to a longer time spent in the faster transient regime at the lower temperature, leading to a higher final mass gain. This is also consistent with TGA results from [1]. This outcome underscores the importance of studying the transient oxidation regime. As no significant spallation has been observed on the samples, the slight decrease in mass at both temperatures was attributed to volatilization. Indeed, the slope of the curve's end is consistent with the Cr_2O_3 volatilization rate shown in [5] at 900 °C (k_v–3.10^{-8} mg·cm $^{-2}$ s^{-1}). If the k_p values were calculated by taken into account the volatilization, their values would be slightly higher. Nevertheless, it remains an hypothesis at this stage. For both temperatures, the two parallelepipedic samples removed at the shortest time exhibited different behaviors; one showed a similar mass gain evolution to that of the flat cylinder sample, while the second one had a significantly lower mass gain due to an apparent shorter transient regime of oxidation.

By utilizing three successive points on the net mass gain curves, it is possible to calculate the parabolic constant of oxidation, k_p, and to track its evolution using the complete parabolic law ($t = A + B\left(\frac{\Delta m}{S}\right) + C(\frac{\Delta m}{S})^2$ with $k_p = \frac{1}{C}$) [6], where t is the time and $\frac{\Delta m}{S}$ is the mass gain per unit surface area. A and B are constants which depends on the transient regime.

The parameters A, B and C were adjusted to fit the evolution of mass gain. The k_p are then plotted on the Arrhenius diagram in Fig. 2 to be compared to the previous TGA experimental data from [1].

The results indicate that the k_p calculated at 900 °C from the data triplet at [0, 1 h, and 16 h] is higher than the k_p found from the SMT-TGA test [1]. This difference can be attributed to the shorter oxidation durations compared to the corresponding step in the SMT-TGA experiment. The k_p values from data triplets at [1 h, 16 h,

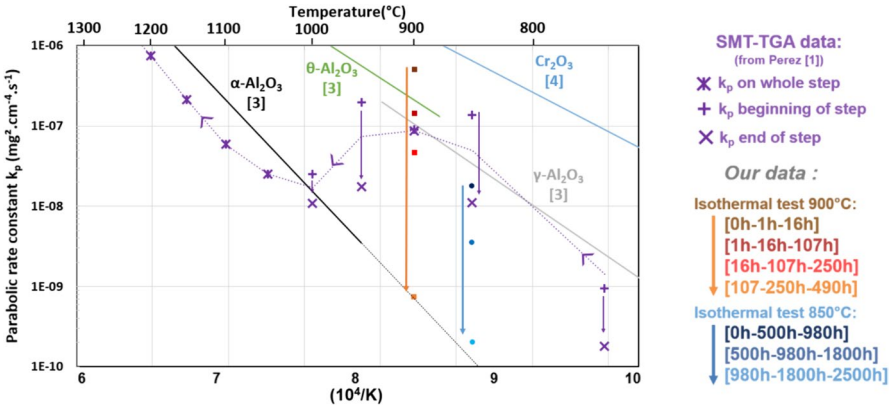

Fig. 2 Arrhenius plot of the parabolic rate constant k_p determined for the AM1 (SMT-TGA in purple). The k_p values for our results (850 °C in blue and at 900 °C in shades of red) were calculated using triplets of points as specified on the right. Oxide reference lines are shown for Al_2O_3 polymorphs on NiAl [3], Cr_2O_3 on Ni-30Cr [4] (Color figure online)

107 h] and [16 h, 107 h, 250 h] align with the data reported by Perez et al. as the durations of oxidation tests are closer. At 850 °C, the durations of the SMT-TGA dwell and the isothermal test conducted in the previous study [1] were much shorter than our experiments. The value obtained in our study can instead be compared to the one obtained in [1] from a 300-h long isothermal TGA at 843 °C (not reported in Fig. 2), which is slightly higher (7.10^{-8} mg^2cm^{-4} s^{-1}) than the one evaluated from the shortest time data triplet [0 h, 500 h, 980 h] at 850 °C.

It is noteworthy that the k_p values obtained for the longest time data triplets, respectively, [107 h, 250 h, 490 h] at 900 °C and [980 h, 1800 h, 2500 h] at 850 °C, reach the values of 7.3×10^{-10} mg^2cm^{-4} s^{-1} and 2.0×10^{-10} mg^2cm^{-4} s^{-1}. The correspondence between these values and the extrapolation values from the curve of the kinetic growth of a pure α-alumina scale formed on β-NiAl is remarkable. Reaching such low k_p values indicates that even at low temperatures, α-alumina is able to fully cover the alloy surface and protect the parts after a sufficiently long duration of oxidation. The k_p values obtained for the shortest time data triplets are in the domain between the typical kinetics of chromia scale growth and those of γ and θ-alumina scale growth. They evolve for intermediate times data triplets towards the kinetics of α-alumina scale growth.az

Low-incidence XRD was performed (after weighing) on the surface of the oxidized flat cylindrical sample. The diagrams are not presented here as they do not allow us to monitor the evolution of the alumina layer that is beneath the superficial transition oxides. Indeed, at 850 °C and 900 °C, the long time spent in the transient regime leads to intense diffraction peaks for all transition oxides. Rutile (Cr,Ti,Ta)O_2 or $CrTaO_4$, spinel $Ni(Al,Cr)_2O_4$, chromia Cr_2O_3, and NiO can be found, but the alumina peaks are mostly hidden or weak. Thus, building correlations between the oxidation kinetics and the XRD analysis is very difficult.

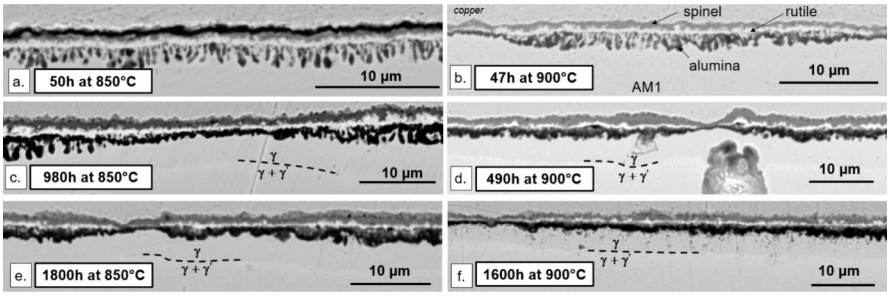

Fig. 3 SEM-BSE micrographs of the oxide layers on AM1 samples after: **a** 50 h at 850 °C, **b** 47 h at 900 °C, **c** 980 h at 850 °C, **d** 490 h at 900 °C, **e** 1800 h at 850 °C, **f** 1600 h at 900 °C

Figure 3 shows the cross sections that are the most representative of the morphology of the oxide layers for each time and temperature. The protective copper layer deposited before sample cutting the cross sections appears light gray on the top. (It is slightly peeled off in Fig. 3a.) EDS analyses were then performed and confirm the presence of the expected oxides: mostly spinel on top in gray with few chromia and NiO, rutile $CrTaO_4$ in white at the metal/oxide interface, and alumina in black under the rutile layer and forming perpendicular internal oxidation precipitates. Under the alumina, the AM1 matrix also appears light gray. A zone depleted in γ' can be observed, and its profile follows the difference in morphology of the alumina precipitates. (The γ/γ' area is slightly brighter than the γ' depleted area.) In this γ'-depleted layer, the little dark spots mostly present for the longest exposure times are titanium nitrides. These latter precipitates mark the non-fully protective character against nitrogen diffusion from air during the transient regime of oxidation. The overall oxide scales are about 3 to 6 µm thick. The oxide layers are the thickest (Fig. 3c,d) at times close to the transition times estimated on the mass gain curves. When the kinetics transition is significantly exceeded, a 0.5 to 2 µm thick alumina layer can be observed. This is consistent with the kinetic drop in the net mass change curve (Fig. 1). Afterward, for longer exposure times (1800 h at 850 °C and 1600 h at 900 °C), the morphology of alumina precipitates changes (Fig. 3e, f) and the spinel layer appears thinner, suggesting a transformation of some spinel and the loss of chromia trough volatilization.

These sample characterizations provide an understanding of the time evolution of the alumina morphology. The alumina initially begins to grow with isolated vertical internal oxidation precipitates, which later merge to form a continuous layer, as shown in Fig. 3b. Intermittently, in sparse areas on most samples,

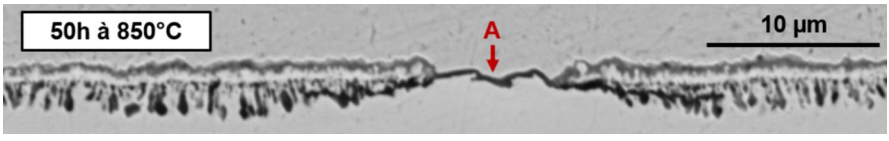

Fig. 4 SEM-BSE micrographs of the oxide layers on AM1 sample after 50 h at 850 °C

even for short times and low-temperature tests, a thin black alumina layer can be observed without any other oxides on top of it (labeled as 'A' in Fig. 4). In these specific areas, we can expect the thin layer to be the most stable and slow-growing α-alumina that formed directly from the start of the oxidation, inhibiting the formation of other oxides. These areas were not correlated with a local chemical variation due to the dendritic structure but rather may be attributed to a grinding scratch.

Photo-stimulated luminescence (PSL) is a characteristic feature of alumina scales containing small amounts of substitutional Cr^{3+} ions. The relative amount of α-Al_2O_3 and θ-Al_2O_3 allotropic structures in the scale were estimated by comparing the intensities of their respective peaks. The θ-Al_2O_3 luminescence is 10–12 times weaker than α-Al_2O_3 according to Tolpygo et al. [7].

Figure 5 summarizes the results from PSL spectra measured across three different samples. The intensity has been calculated by multiplying the intensity of θ peaks by a factor of 10 in order to compensate for the weaker photoluminescence of θ compared to α. We can clearly see the evolution of the alumina from the θ structure to the more stable α structure. In fact, for shorter exposure times and lower temperatures, we find almost only θ-alumina (95% for 50 h at 850 °C). As the oxidation time or temperature increases, the proportion of θ-phase decreases in favor of α-phase. We reach a 50/50 ratio for 1800 h at 850 °C. The PSL spectroscopy confirms the hypothesis made about isolated area A in Fig. 4 with only α-alumina (bold gray line). These analyses demonstrate that both alumina structures can be present even at 850 and 900 °C for hundreds of hours; at these temperatures, the θ structure forms in the majority, and then, it transforms over time to the α structure. Increasing the temperature accelerates the transformation of alumina. The observations are consistent with Martin et al. on the same alloy [2].

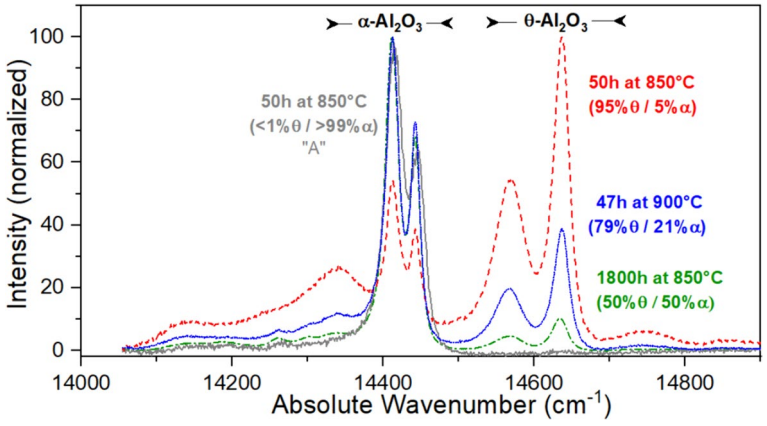

Fig. 5 PSL spectra of cross sections of oxidized AM1 (3 s acquisition per spot): the red, blue, and green curves are the average of 5 spectra taken in random places within the alumina layer, and normalized to the highest peak. The gray curve is a single normalized spectrum of a spot taken in area A (see Fig. 4) (Color figure online)

Discussion

The model proposed by Perez et al. [1] for AM1 oxidation kinetics is now discussed in light of the present results at 850 °C and 900 °C. The model has been constructed using some simplifications. It considers only two types of oxides growing on the alloy, with two different oxidation kinetics constants: the transient oxides (k_{p1}) which include here spinels, rutile, localized chromia and internal transient alumina, and α-alumina (k_{p2}). It is assumed that the rapid oxidation regime is due to the parabolic growth of a covering layer made of transient oxides at the surface of the alloy and of some internal transient alumina. Underneath this layer, randomly distributed precipitates of α-alumina begin growing from the start of the oxidation, increasing both thickness and lateral extent. At the sites of these precipitates, the growth of the oxide layer is controlled by the diffusion of elements through the α-alumina precipitates, resulting in a considerable slowdown in the growth of the transition oxides above the precipitates. Therefore, in the model, the transition oxide layer above an alumina precipitate is considered to no longer grow once the alumina has fully covered the alloy surface. Hence, the third parameter of the model describes the lateral growth kinetics of internal alumina precipitates. The logic of the model, involving randomly distributed nuclei on an initial surface and linear growth of the radius of these nuclei, is adapted from Evans et al. [8]. The equations of this oxidation kinetics model are provided below, sourced from [1]. The mass gain per unit surface area at the time i, of transient oxide $\Delta m1_i$ on top of a surface without alumina precipitate is given by Eq. 1.

$$\Delta m1_i = \sqrt{m_0^2 + k_{\mathrm{p1}} \times t_i} \tag{1}$$

$$\Delta m2_i = \sqrt{k_{\mathrm{p2}} \times t_i} \tag{2}$$

$$\theta_i = 1 - e^{-k_t \times (t_i + t_0)^2} \text{ with } t_0 = \frac{m_0^2}{k_{p1}} \tag{3}$$

where t_i is the time from beginning of the dwell, m_0 is the mass gain during the heating process, and k_{p1} is the parabolic constant corresponding to the thickening of the transient oxides. The mass gain per unit surface area at the location of α-Al_2O_3 precipitates $\Delta m2_i$ is given by Eq. 2, with k_{p2} the parabolic constant corresponding to the thickening of α-Al_2O_3. The coverage of the metal surface by α-Al_2O_3, called θ, is given by Eq. 3 with k_t a thermally activated parameter characterizing the kinetics of spreading of α-Al_2O_3 and t_0 the time needed to form the same mass gain during the high temperature dwell as the mass gain m_0 during heating. t_0 allows to take into account the advancement of the transition during the heating process. The mass gain over time is then calculated by incrementing the time from the beginning of the isothermal stage with equation Eq. 4.

$$\Delta m_i = \Delta m_{i-1} + \left(\Delta m1_i - \Delta m1_{i-1}\right) \times e^{-k_t \times \left(t_i + t_0\right)^2} + \left(\Delta m2_i - \Delta m2_{i-1}\right) \times \left(1 - e^{-k_t \times \left(t_i + t_0\right)^2}\right) \tag{4}$$

where i is the time increments and Δm_i is the total mass gain per area at the time step i. To summarize, the input parameters of the model are only 4: m_0, k_{p1}, k_{p2}, and k_t, or 7 if we consider that the 3 kinetics constants follow Arrhenius laws. In [1], values for these parameters have been determined from experimental oxidation tests and have well reproduced oxidation kinetics across a large range of temperatures and times. The results of long isothermal oxidation at 850 °C and 900 °C allow for slight adjustments to the kinetic parameters of the model (Eqs. 5–7) to more accurately fit the AM1 oxidation behavior at low temperatures.

$$k_{p1} = 3.1 \times 10^7 \times e^{\frac{-3.1 \times 10^5}{R \times T}}\ mg^2 cm^{-4} s^{-1} \tag{5}$$

$$k_{p2} = 7.1 \times 10^8 \times e^{\frac{-4.2 \times 10^5}{R \times T}}\ \mathrm{mg^2 cm^{-4} s^{-1}} \tag{6}$$

$$k_t = 2.8 \times 10^{24} \times e^{\frac{-8.0 \times 10^5}{R \times T}}\ \mathrm{s^{-2}} \tag{7}$$

A first convenient way to examine the results obtained from the model is through a time–temperature diagram (Fig. 6). In this figure, the lines represent the oxidation time needed to transition from the transient regime to the stationary α-alumina regime calculated by the model. The criteria for the change of oxidation regime are chosen to be when the mass of oxygen fixed by the transition oxides during a time step increment is less than 10% of the mass of oxygen fixed by the growth of α-alumina. The dashed lines represent the results of the model with parameter values from [1], while the continuous lines represent the results with new parameter values given above. Thus, all oxidation test conditions (time and temperature) to the

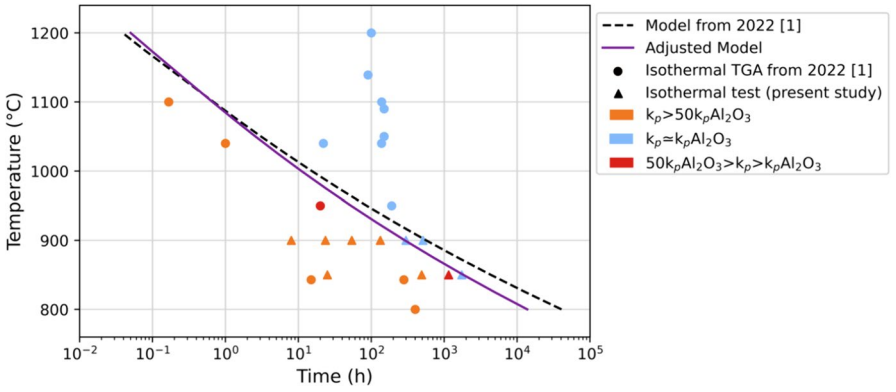

Fig. 6 Time–temperature diagram of AM1 transient regime (2022 model by Perez et al. [1] and adjusted model)—the bold line (the transition) corresponds to the moment where the net mass gain of the transient oxides = 10% of the net mass gain of Al_2O_3

right of the transition line in the diagram are predicted by the model to correspond to the growth of a continuous protective α-alumina layer. The results of the model can be compared to the experimental data depicted by the symbols in Fig. 6. The isothermal tests using TGA from Perez et al. study [1] are referenced with round dots. The oxidation tests of the present study are referenced with triangles. The color of symbols (orange or blue) indicates in which range, and the corresponding k_p values stand compared to the value taken from the reference k_p for α-Al_2O_3. The k_p value used here are the final ones evaluated from the local k_p analysis of the TGA experiments, and the ones evaluated from time triplet data values for box furnace oxidation tests of the present study. For the latter, the k_p values are attributed to the time taken in the middle of the triplet interval. The transient regime is considered to be when k_p is larger than 50 times the k_p of α-Al_2O_3 [3]. The stationary regime is considered for k_p close to the k_p of α-Al_2O_3. The red color is applied in the in between situation.

At 850 °C and 900 °C, the k_p values meet the criteria set for the transition for shorter times than those predicted by the model with parameters taken from [1]. From the slight tilt between the two lines, it can be observed that the newly adjusted parameters (given in Eq. 5–7) allowed for a better simulation of the oxidation behavior of AM1 at low temperatures without significantly altering the results at higher temperatures. Hence, the study of long isothermal oxidation allowed for the global validation and slight adjustment of the AM1 kinetics model of oxidation across a very large range of temperatures and times.

In the model, θ-Al_2O_3 is categorized with the transition oxides, which are assumed to grow with kinetics described by k_{p1}. The fact that a portion of the transition oxides is θ-Al_2O_3 has no significant impact on the kinetics predicted by the model. However, it is important to differentiate between the allotropic forms of alumina when comparing the morphology of the oxide scale in cross section with the α-Al_2O_3 surface coverage predicted by the model (Eq. 3), as shown in

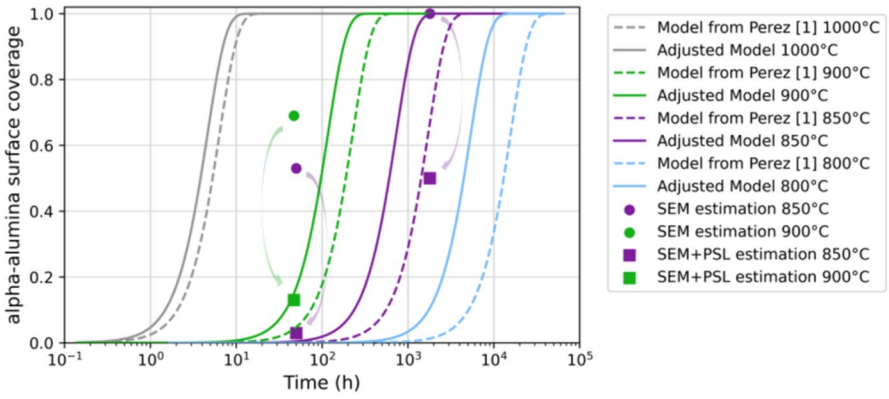

Fig. 7 Variation of surface coverage α-alumina from 0 to 1 (= full coverage) as a function of time (model from 2022 *vs* adjusted model). The dots correspond to an experimental estimation of the coverage done by SEM. The squares are an estimation combining SEM observations and PSL spectroscopy which allow α-Al_2O_3 identification

Fig. 7. Indeed, at lower temperatures and shorter exposure times, most of the dark areas seen in cross sections are θ-Al_2O_3. Even though they may appear similar to α-Al_2O_3 in the SEM, these areas should be excluded from the estimation of the surface coverage. Thus, by combining SEM estimations of the continuity of the alumina layer (picture analysis of the dark areas in Fig. 3) with relative quantities of α-Al_2O_3 from θ-Al_2O_3 obtained by PSL in Fig. 2, we are able to compare our experimental data with the α-Al_2O_3 surface coverage predicted by the model. Figure 7 shows the estimations of the surface coverage by alumina performed by the SEM only, which includes both α-Al_2O_3 and θ-Al_2O_3 (dots), and more accurate estimations obtained by combining the previous SEM coverage estimations with the PLS relative quantities of α-Al_2O_3 (square symbols). As it is challenging to carry out such a hybrid accurate analysis, it has been performed only on three samples. The two experiments with short oxidation times show good agreement with the adjusted model (lines) and the data (square symbols). However, the longest duration experiment, showing a 50% coverage of α-Al_2O_3 after 1800 h at 850 °C, estimates the α-Al2O3 surface coverage to be slightly lower than expected from the adjusted model. The cross section of this sample in Fig. 3e**,** representative of the entire surface, shows a continuous layer of alumina, but it is possible that α-Al_2O_3 already forms a thin continuous layer with precipitates of θ-Al_2O_3 below or above it. Thus, for a relative quantity of α-Al_2O_3 large enough (found by PSL spectroscopy), α-Al_2O_3 layer continuity might be reached, even though spectra still show θ-Al2O3 in the cross sections. Consequently, for long oxidation times, the hybrid estimation of coverage (SEM/PSL) loses its accuracy, and we can assume from the cross sections that the quantity of α-Al2O3 is sufficient to form a continuous layer (surface coverage > 99%). Therefore, the model adjustment seems to fit well with the experimental data.

Another way to visualize the improvement of the model is to plot the predicted net mass gain curve obtained with the newly adjusted kinetic parameters and compare it with the experimental data and the predictions from the previous model. Figure 8 illustrates this comparison, where the upper and lower limits (dashed lines) represent the consequences of the uncertainty level of the kinetic parameters (k_{p1}, k_{p2}, k_t).

The availability of new data at lower temperatures led to a decrease in the duration of the transient regime and consequently the final mass gain. It also resulted in a slight narrowing of the confidence interval of the model. The experimental net mass gains align well with the adjusted model, with the exception of one sample at each temperature, which is close to the lower limit of the adjusted model. This variability could be attributed to some heterogeneous grinding of these two samples. Indeed, as demonstrated by Sudbrack et al. [9] at 815 °C, a rougher surface finish promotes the formation of α-alumina, affecting the oxidation kinetics. It is likely that these two samples were ground more vigorously on their lateral surfaces due to their smaller size. The phenomenon is under study. It was observed (not shown here) that the lateral surfaces formed α-alumina faster than the main surfaces. Grinding leads to an increase of dislocation density leading to a faster diffusion at low temperatures, and the stored elastic energy may favor the nucleation of the most stable phase, α-alumina.

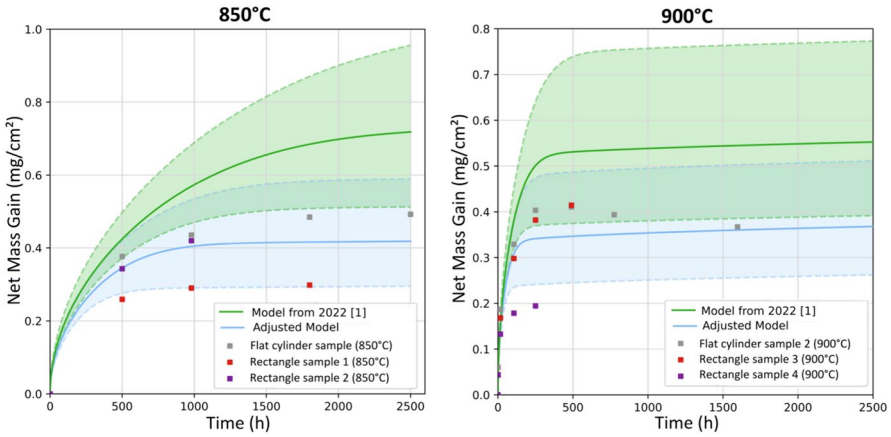

Fig. 8 Net mass gain curves (model from 2022 and adjusted model) with the areas of uncertainty of the 3 kinetic parameters

Conclusions

The objective of this study was to deepen the understanding of the oxidation behavior of the Ni-based superalloy AM1 at 850 °C and 900 °C using long isothermal tests. The existence of a transient oxidation regime led Perez et al. to develop a model that incorporates this transient regime to predict oxidation kinetics at any time and temperature. This study aimed to address the lack of data at lower temperatures (< 1000 °C) and for much longer durations. The model predicted that, in this intermediate temperature range, after a very long transient regime, slow kinetics controlled by α-alumina scale growth would be reached. However, this had never been experimentally proven before the present work. The long-term experiments conducted here at 900 °C and 850 °C demonstrated that bare AM1 alloy can be classified as an alumina-forming alloy even in this lower temperature domain but for sufficient oxidation durations. The durations of the transient regime were found to be 1500 h at 850 °C and 250 h at 900 °C, slightly shorter than predicted by the previously published set of parameters of the model [1]. An adjustment of the model was carried out, showing some noticeable improvement. As noted by Perez et al., samples oxidized for short times exhibit (on SEM cross sections) an interface with more alumina than expected from the model prediction. New results obtained in this study show that a part of this alumina layer is θ-alumina. PSL spectroscopy identified a majority of θ-alumina within the internal alumina layer at 850 °C and for short exposure times, confirming the observations of Martin et al. [2]. The distinction between α and θ-alumina has no influence on the kinetics parameters of the model, as θ-Al_2O_3 is categorized with the transition oxides due to similar growth rates. The formation of a continuous α-Al_2O_3 layer remains the sole trigger for drops in oxidation kinetics. However, evaluating the relative amounts of α and θ is necessary to correlate the experimental α-Al_2O_3 surface coverage with the model's prediction. After slight adjustments at low temperatures, the entire set of experimental data and

the model show good agreement. The variability in mass gain at each temperature among the three tested samples suggests thatstresses induced by rougher surface preparation promote early formation of

Acknowledgements This study was performed thanks to the financial support of Safran Tech. The AM1 alloy was provided by Safran Aircraft Engines.

Author Contributions Martin Batiste contributed to experimental work and writing of the first draft and prepared the figures and tables; Thomas Perez was involved in experimental work, kinetic modeling, and research funding; Tom Sanviemvongsak contributed to research funding; Clara Desgranges was involved in research funding when at Safran Tech and participation to kinetic modeling; Daniel Monceau contributed to original idea, bases of kinetics modeling, and coordination; and all authors were involved in discussion of the results, ideas, and reviews of the manuscript.

Funding Open access funding provided by Institut National Polytechnique de Toulouse. Funding was provided by Institut National Polytechnique de Toulouse, Safran Tech, CEA, CNRS.

Data Availability No datasets were generated or analyzed during the current study.

Declarations

Competing interests The authors declare no competing interests.

References

1. T. Perez, D. Monceau, and C. Desgranges, *Corrosion Science* **206**, 2022 110485.
2. A. Martin, J. Cormier, J. Rame, E. Drouelle, and F. Pedraza, *Corrosion Science* **229**, 2024 111872.
3. M. W. Brumm and H. J. Grabke, *Corrosion Science* **33**, 1992 (1677).
4. X. Huang, L. Martinelli, S. Bosonnet, P. C. M. Fossati, L. Latu-Romain, and Y. Wouters, *Oxidation of Metals* **96**, 2021 (69–80).
5. Hänsel, M. Korrosions und Kompatibilitätsstudien and CrBasislegierungen für den metallishen Interkonnektor der Hochtemperaturbrennstoffzelle, Diss. RWTH Aachen, Jül-3583 (1998), ISSN 0944–2952
6. D. Monceau and B. Pieraggi, *Oxidation of Metals* **50**, (5/6), 1998 (477).
7. V. K. Tolpygo and D. R. Clarke, *Materials at High Temperatures* **17**, 2000 (59–70).
8. U. R. Evans, *Transactions of the Faraday Society* **41**, 1945 (365–374).
9. C. K. Sudbrack, D. L. Beckett, and R. A. MacKay, *JOM* **67**, 2015 (2589–2598).

Authors and Affiliations

Martin Batiste[1] · Thomas Perez[2] · Tom Sanviemvongsak[2] · Clara Desgranges[2,3] · Daniel Monceau[1]

✉ Daniel Monceau
daniel.monceau@toulouse-inp.fr

Martin Batiste
martin.batiste@toulouse-inp.fr

Thomas Perez
thomas.perez@safrangroup.com

Tom Sanviemvongsak
tom.sanviemvongsak@safrangroup.com

Clara Desgranges
clara.desgranges@cea.fr

[1] CIRIMAT Laboratory, University of Toulouse, ENSIACET, 4 allée Emile Monso, BP 44362, 31030 Toulouse Cedex, France

[2] Safran Tech, Rue des Jeunes Bois, Châteaufort, CS 80112, 78772 Magny-Les-Hameaux, France

[3] Present Address: CEA-Saclay, Saclay, France